



GRACE grant no 679266

Submission of presentation to conferences

D4.4

WP4: Combat of oil spill in coastal arctic water - effectiveness and environmental effects



Prepared under contract from the European Commission
Contract n° 679266
Research and Innovation Action
Innovation and Networks Executive Agency
Horizon 2020 BG-2014-2015/BG2015-2

Project acronym: GRACE
Project full title: Integrated oil spill response actions and environmental effects
Start of the project: 01 March 2016
Duration: 42 months
Project coordinator: Finnish Environment Institute (SYKE)
Project website: <http://www.grace-oil-project.eu>

Deliverable title: Submission of presentation to conferences
Deliverable n°: D4.4
Nature of the deliverable: Report
Dissemination level: Public

WP responsible: WP4
Lead beneficiary: AU

Due date of deliverable: 28th February 2019
Actual submission date: 28th February 2019

Deliverable status:

Version	Status	Date	Author	Approved by
1.0	draft	26 th February 2019	Chris Petrich Nga P. Dang Janne Fritt-Rasmussen Kim Gustavson	Kim Gustavson, WP4 leader
2.0	final	28 th February 2019	Chris Petrich Nga P. Dang Janne Fritt-Rasmussen Kim Gustavson	Steering group

Table of Content

Executive summary.....	4
41nd AMOP Technical Seminar on Environmental Contamination and Response, 2018, Vancouver, British Columbia, Canada (Platform presentation).....	5
Laboratory In-situ Burns of Oil on Ice	5
Abstract	5
Introduction.....	5
Methods.....	5
Results.....	6
Discussion	7
Conclusion.....	8
Acknowledgements.....	9
References	9
Figures.....	10
Tables.....	14
Supplementary information.....	15
Background	15
Methods.....	15
Oil Residue	20
Results and Discussion.....	20
Lessons Learned for Main Experiments	23
References	23

Executive summary

Oil spills in ice-covered waters pose unique challenges to remediation activities. In-situ burning is a potential remediation technique that has shown promising efficiency in earlier trials. An element of arctic in-situ burning is the feedback between the flame of a burn on oil-infiltrated sea ice and the melting ice beneath.

This deliverable presents a conference paper, which was submitted in 2018 for the 41nd AMOP Technical Seminar on Environmental Contamination and Response, 2.-4. October 2018, Vancouver, British Columbia, Canada. At the conference the paper was presented as a platform presentation.

The conference contribution covered experiments carried out as a series of experiments, which were devised to quantify the impact of this mechanism on burn efficiency. Seven experiments were performed that started with a crude oil pool of 0.2 or 0.3 m diameter on a 1 x 1 m² freshwater ice block. The pools were ignited and the development of the flame, ice temperatures, and ablation rates was monitored. All burns ended in a vigorous burn phase (boil-over). Burn efficiency was below 65%. A simple pond spread model was used to derive burn rates of a spreading pond. Burn rates were mostly around 0.9 mm/min. The low burn efficiencies were found to result from significant increase of the pond area during the burn in combination with relatively thin initial oil pools. The measurements provide a starting point to address the feedback effect of pond spread and ablation on burns on an oil-infested sea ice surface layer.

41nd AMOP Technical Seminar on Environmental Contamination and Response, 2018, Vancouver, British Columbia, Canada (Platform presentation)

Laboratory In-situ Burns of Oil on Ice

Chris Petrich¹, Nga P. Dang¹, Janne Fritt-Rasmussen², Kim Gustavson²

¹Northern Research Institute Narvik (Norut Narvik), Norway

²Aarhus University, Roskilde, Denmark

Abstract

Oil spills in ice-covered waters pose unique challenges to remediation activities. In-situ burning is a potential remediation technique that has shown promising efficiency in earlier trials. An element of arctic in-situ burning is the feedback between the flame of a burn on oil-infiltrated sea ice and the melting ice beneath. A series of experiments was devised to quantify the impact of this mechanism on burn efficiency. Seven experiments were performed that started with a crude oil pool of 0.2 or 0.3 m diameter on a 1 x 1 m² freshwater ice block. The pools were ignited and the development of the flame, ice temperatures, and ablation rates was monitored. All burns ended in a vigorous burn phase (boil-over). Burn efficiency was below 65%. A simple pond spread model was used to derive burn rates of a spreading pond. Burn rates were mostly around 0.9 mm/min. The low burn efficiencies were found to result from significant increase of the pond area during the burn in combination with relatively thin initial oil pools. The measurements provide a starting point to address the feedback effect of pond spread and ablation on burns on an oil-infested sea ice surface layer.

Introduction

In-situ burning of oil on ice is a potential spill remediation technique in the Arctic (Buist et al., 2013). Investigations have been performed of feedbacks from a flame on vertical ice walls, for example in ice cavities and at the edge of leads (e.g., Bellino et al., 2013; Farahani et al., 2017; Shi et al., 2017). However, there seems to be only one estimate of the downward heat flux through an oil slick into underlying water, finding 2.5 kW/m² (Evans et al., 1988). Sea ice has been found to contain up to 5% oil in its pore structure (NORCOR, 1975), so a downward heat flux from a burning oil pool may result in the release of oil during in-situ burning on oil-infested sea ice. The energy balance of a burn is comprised of evaporation and combustion linked by radiative and conductive heat transfer (Buist et al., 2013). The goal of this work was to quantify how the burning pool affects the ice surface. Experiments were performed on freshwater ice to facilitate the quantitative analysis.

Methods

Burns of a shallow pool of oil were performed in an ice-filled pan on the Roskilde campus of Aarhus University (Figure 1). Ice was grown from freshwater in tapered stainless-steel pans, approx. 1 m x 1 m x 0.25 m in size. To accommodate expansion of the ice, the walls of the pan were lined with foam on the inside which was separated from the water by a tarp. A vertical temperature probe with K-type thermocouples was placed at the center of the pan. A silicone mould of diameter 200 or 300 mm was placed at the water surface in the center to provide a template for the initial oil pool. The prepared pan was placed on a palate and frozen in cold room at -15 °C.

Burns were performed outdoors in a partially shielded enclosure to reduce the effect of winds and prevent environmental contamination (Figure 1). The silicone mould was removed, thermocouples were connected to the logger, and naphthenic North Sea crude oil was poured into the pool shortly before ignition. The temperature of the oil was ambient temperature (Table 1). Oil was ignited with a blow torch. The burn was recorded by a video camera. Flame dimensions (width at the base of

the flame and height) were determined automatically from frame capture images ten times per second. The flame was identified by pixel color and brightness (Figure 2).

Temperatures were recorded in 5 mm intervals through the oil pool and ice and 300, 600, and 900 mm above the oil pool, i.e., in the flame. A Campbell Scientific CR1000 logger recorded temperatures and data from a weather station during the burns. The sensible heat of the ice was calculated by multiplying the ice temperatures with heat capacity 2100 J/kg K, ice density 920 kg/m³, and separation of thermocouples 5 mm.

Prior to and after each burn, ice surface profiles were measured along two perpendicular transects to determine ablation. Following each burn, the oil residue was collected through a combination of mechanical recovery and oil absorbent pads, both from the pool and the ice surface. The absorbent pads were pre-weighted, and the burn efficiency was determined from the ratio of collected residue mass to mass of the oil at the start (Table 1).

The volume of surface ablation was estimated from the two perpendicular transects. For this, an ablation profile was calculated by subtracting the pre-burn profile from the post-burn. Working in cylindrical coordinates with respect to the center of the original oil pool, each ablation profile was assumed to be characteristic for half of the ice surface. The corresponding enthalpy was determined by multiplying the ablated volume with ice density $\rho=920$ kg/m³ and latent heat of fusion of ice $L=334$ kJ/kg (Table 2).

The burn rate (i.e., oil regression rate) is typically specified as a volume flux in mm/min. In the present experiments, the burn rate, v , was estimated from initial oil pool dimensions, burn time, and burn efficiency, assuming a constant rate of spread of the linear dimension of the oil pool, w . The surface area of the pool at time t after ignition was thus

$$A(t) = \frac{\pi}{4} (d_0 + wt)^2$$

[1]

where w is the rate of increase of the diameter of the pool, t time since start of the burn, and d_0 the initial diameter of the pool. The instantaneous rate of change of oil volume V was

$$\frac{dV}{dt} = -A(t) v$$

[2]

which can be integrated to obtain an expression for the remaining oil volume

$$V(t) = V(0) - \frac{\pi v}{12w} [(d_0 + wt)^3 - d_0^3]$$

[3]

where $V(0) = h(0) A(0)$ is the initial volume of oil. The oil slick thickness h and burn efficiency ε are found from Equations [1] and [3] as

$$h(t) = \frac{V(t)}{A(t)}$$

[4]

and

$$\varepsilon(t) = 1 - \frac{V(t)}{V(0)}$$

[5]

Parameters v and w were fitted to a system with initial conditions d_0 , $h(0)$, burn time t_x , and final conditions $h(t_x)=1.5$ mm and $\varepsilon(t_x)$. No explicit allowance was made for changing burn rates during the initial growing phase of the flame, the vigorous burn phase, or based on oil slick thickness. The initial oil volume was derived from the original oil mass with a density of 845 kg/m³.

Results

Between 350 and 800 g of crude oil were burned in pools of 0.2 or 0.3 m diameter, corresponding to between 8 and 27 mm initial oil thickness (Table 1). Successful burns took between 230 and 320 seconds and ended with a vigorous burn phase (boil-over). Two burns were classified as unsuccessful when oil moved along or ran off the ice surface through cracks in the ice (171024 and 171116-1). Burn efficiencies ranged between 35 and 64% by mass, and the residual oil floated on the meltwater pool. The amount of oil splattered around the pool was insignificant.

The development of a burn is illustrated in Figure 3 and quantified in Figure 4. The fire developed within the first 30 seconds from which point on it increased slowly in diameter and height. The typical maximum flame height was 1.0 m. The flame height was between 1 and 2 to 3 times the flame diameter during most of the burn period and the ratio decreased toward the end of the burn when the oil pool diameter spread considerably without a proportional increase in flame height. Due to winds, the ratio was below 1 around 75 seconds from the beginning of burn 180321-1 (Figure 4b). The vigorous burn phase is most readily discernable in burn 180321-1 (Figure 4b) where the flame height rapidly increased beyond 1.4 m (i.e., beyond the field of view of the camera). The vigorous burn phase is less obvious in the graphs of burns 171115-2 and 180321-2 where it appears to follow a (subtle) temporary reduction in flame height. However, flame brightening, increased volume, and ejected droplets were apparent during the vigorous burn (not visible in Figure 4). Figure 4c shows the presence of a small flame following the vigorous burn phase which is an experimental artifact due to wicking at the cables of the temperature probe.

The flame width increased initially to fill the oil pool before growing at a constant rate. Lateral extent accelerated after about 3 minutes in burns 171115-2 and 180321-1. The apparently near-constant rate of increase in diameter between 50 and 150 s was between 3 and 6 cm/min (Table 2). According to the interpolated line, the flame width at 50 s was 18, 29, and 28 cm, respectively, in agreement with the initial oil pool diameters of 0.2, 0.3, and 0.3 m, respectively. The average flame height increased at a rate of 8 to 10 cm/min during the period from 50 to 150 seconds.

The flame spread predominantly in the direction of maximum ice surface slope, i.e. perpendicular to the line of sight in burns 171115-2 and 180321-1, and parallel to the line of sight in 180321-2.

The fitted pool spread rate was approx. 6 cm/min in all burns (Table 2) and corresponds to final pool diameters between 45 and 58 cm. The estimated burn rate was 0.8 to 1.0 mm/min in three burns between 14 and 27 mm initial pool depth, and 0.4 mm/min in two burns of 8 and 12 mm initial pool depth (Table 2). The burns with low burn rate had also the lowest burn efficiency.

Ice surface profiles are shown in Figure 5. The initial profiles tended to be slightly sloped in one direction, and ablation was skewed toward the downward direction. Ablation perpendicular to the slope was symmetric. The camera faced north, i.e. the flame width indicated in Figure 4 corresponds to the East-West ablation profile in Figure 5. Ablation was highest along the axis of surface slope. The total estimated ablation was fairly consistent between burns, ranging from 2500 to 3000 cm³, corresponding to 750 to 1000 kJ (Table 2).

The thermocouple nominally at the ice–air interface melted out within the first 1 to 3 minutes of the burns of 21 Mar 2018. The thermocouple nominally 5 mm lower reached 0 °C at the end of the burn. Within the accuracy of the vertical placement of the thermocouples it can be concluded that approximately 5 mm of ice melted in burns 180321-1 and -2, and less than 5 mm in burn 171115-1 directly beneath the original oil pool. The sensible heat flux into the ice that resulted in ice warming ranged from 10 to 950 W/m² (Table 2). Burn 171115-2 started with ice temperatures near 0 °C, explaining the absence of a heat flux. The lowest initial ice temperatures (< -5 °C) existed in burn 180321-2, which also shows the greatest sensible heat flux.

Discussion

Burn efficiency was low compared with 85 to 98% generally expected for light to medium crude oils (Fingas, 2016). We showed that the observed burn efficiencies <65% can be plausibly explained by accounting for the lateral spread of the oil pool as the surface was melting combined with the comparatively thin initial oil layer thickness (Table 2). Based on an assumed final oil film thickness of 1.5 mm, the burn efficiency of a 15 mm thick oil pool that does not spread would have been 90%. However, the burn efficiency would have been only 56% if the pool started with 0.2 m diameter, the diameter increased at a rate of 6 cm/min, and the burn rate was 0.9 mm/min. The final pool area would have been 4.4 times the original area.

Spread is a concern for pools that increase their area significantly. For example, in in-situ burn experiments on Svalbard (Dickins et al., 2006), an initial area of 69 m² (i.e., equivalent pool diameter 9.4 m), film thickness of 35 mm, burn time of 11 minutes, final thickness of 1 mm, and burn efficiency of 96% were reported. With these constraints, the fitted parameters would be burn rate of $v=2.6$ mm/min and pool spread of $w=16$ cm/min. The fitted burn rate is at the lower end of the expected 3 to 4 mm/min for pools of this size (Buist et al., 2013). The resulting final pool area just shy of 100 m² is compatible with the reported description that “oil spread out and filled the approximate 100 m² melt pool”. The impact of lateral spread of less than a factor of two on burn

efficiency was minor. The burn efficiency would have been 87% had the pool spread to an area 4.4 times its original area.

Combined, it appears plausible that the low burn efficiencies in the current experiments resulted from a significant increase of the pool diameter during the burn aggravated by a thin initial oil pool. The order of magnitude of the sensible heat flux into the ice, i.e., around 700 W/m^2 , is consistent with expectations for an ice interface at its melting point. Ablation beneath the original oil pool was small (5 mm of a 0.2 m diameter pool are 160 cm^3) compared with the total ablated volume (2500 to 3000 cm^3). This indicates that a noticeable amount of oil may be released from the near-surface layers during an in-situ burn of oil-infested sea ice. Dividing the enthalpy due to melt by burn time and the average area of the oil pool during the burn time (based on w , Table 2), one finds an average heat flux that induced melt of 42, 19, and 30 kW/m^2 in burns 171115-1, 180321-1, and 180321-2, respectively. 30 kW/m^2 is sufficient to melt 6 mm of ice per minute. If the ice is permeated by 5% oil (NORCOR, 1975), then an oil layer of 0.3 mm thickness could be released per minute. This is at the low end of the lowest burn rates determined in this study and thus not sufficient to sustain the burn. However, it would extend the amount of oil burned measurably (>30%). The question of how this flux scales with pool size and develops over time remains to be addressed.

The increase of the pool area could not be assessed accurately based on the video recordings since the pool spread predominantly in one direction (either perpendicular or parallel to the direction of view of the camera). Hence, the apparent acceleration of the pool size in burns 171115-2 and 180321-1 is difficult to interpret (Figure 4).

Errors exist in the presented method of estimating surface ablation due to the directional spread of the pool. The final surface profile perpendicular to the slope passed through the original flame center which was offset from the final center of the flame. However, while the ablation estimate in direction of slope was an overestimate, the estimate perpendicular was underestimate, compensating the error of the former to some degree. However, non-systematic (i.e., random) imperfections of the ice surface should contribute to scatter in the results.

The model is based on volumetric efficiency (Eqn. 5) while measurements are given as efficiency by mass (Table 1). In this presented calculation it was assumed that the density of the final product was equal to the density of the fresh crude oil. However, the density may have been up to 15% higher without causing the oil to sink. In that case the derived values for w would have been up to 1 cm/min lower and those of v 0.1 to 0.2 mm/min higher than given in Table 2.

The low burn rates of experiments 171116-2 and 180321-2 are yet to be explained. The burn rate was assumed constant in the model although it is known to depend on pool thickness and diameter (Garo et al., 1999; Buist et al., 2013). The spread of the pool had been similar across the experiments. It has been reported that oil pools of thickness below 5 mm burn substantially slower than pools thicker than 10 mm (Buist et al., 2013), and the two burns with low burn rates happen to have been the ones with the thinnest initial oil pools. Experiments of Garo et al. (1999) showed decreasing burn rates for initial pool thicknesses below 8 mm. In pools of 0.23 m diameter, the burn rate ranged from 0.5 mm/min at 2 mm initial thickness to 0.8 mm/min above 10 mm initial thickness. The corresponding burn rates at 0.5 m diameter were 1.0 and 1.3 mm/min, respectively. However, more specific characterizations of the burn rates and more detailed characterizations of the pool spread would be necessary to assess this effect quantitatively. However, those data do not explain the observed differences. This aspect needs to be investigated further.

Conclusion

Experiments were conducted with the aim of quantifying the feedback between a burning oil pool and oil-infested sea ice. In this study, burn experiments were conducted on freshwater ice with all oil initially concentrated in a pool, and the pool allowed to spread in response to surface melt. The feedback effect between a burning pool on top of oil-infested sea ice remains to be quantified as does upscaling to full-scale in-situ burns, but it was shown that the spreading pool has the potential to accumulate a significant amount of near-surface oil.

It was found that three of five burns had a burn rate in the expected range for pools of this size (i.e., 0.7 to 1.0 mm/min), while two burns had burn rates notably smaller (0.4 mm/min). The reason for the difference is currently not clear, and the thickness of the initial oil slick remains a candidate. Burn efficiencies were low compared with previous reports (<65% vs. >85%). However, it was found that the low efficiencies are explained by a simple oil burn and pool spread model, and that

they are a systematic consequence of allowing the pool to spread combined with a comparatively thin initial oil pool.

The way to maximize burn efficiency is to avoid the lateral spread of an oil layer (i.e., $w=0$). This can be accomplished on sea ice for example by constructing compacted snow berms surrounding the burning pool (Owens et al., 2017). However, spread may be difficult to avoid in large-scale in-situ burns where engineering attention cannot be paid to individual ponds. This work lays to the foundation to upscale feedback effects due to melt to full-scale burns.

Acknowledgements

This project has received funding from the European Union's Horizon 2020 research and innovation programme under grant agreement No 679266 (GRACE).

References

Bellino, P., M. Flynn, and A.S. Rangwala. "A study of in-situ burning of crude oil in an ice channel." *Proceedings of the Combustion Institute* 34(2): 2539–2546, 2013.

Brogaard, N.L., M.X. Sørensen, J. Fritt-Rasmussen, A.S. Rangwala, G. Jomaas. "A new Experimental Rig for Oil Burning on Water – Results for Crude and Pure Oils." In *Proceedings of the 11th International Symposium for Fire Safety Science, IAFSS, Christchurch, NZ, 2014*. 14 pp, 2014.

Buist, I.A, S.G. Potter, B.K. Trudel, S.R. Shelnut, A.H. Walker, D.K. Scholz, P.J. Brandvik, J. Fritt-Rasmussen, A.A. Allen, and P. Smith. "In Situ Burning in Ice-Affected Waters: State of knowledge report. Final report 7.1.1." Report from Arctic Oil Spill Response Technology Joint Industry Programme (JIP). 294 pp., 2013.

Dickins, D., P.J. Brandvik, L.-G. Faksness, J. Bradford, and L. Liberty. "2006 Svalbard Experimental Spill to Study Spill Detection and Oil Behavior in Ice." Final Technical Report. United States Department of Interior Minerals Management Service, 94 pp, 2006.

Evans, D.D., G. Mulholland, D. Gross, H. Baum, and K. Saito. "Burning, Smoke Production, and Smoke Dispersion from Oil Spill Combustion". In *Proceedings of the Eleventh Arctic and Marine Oilspill Program (AMOP) Technical Seminar, June 7-9, Vancouver, BC*. Environment Canada, Ottawa, ON, Canada, pp. 41-87, 1988.

Farahani, H.F., W.U.R. Alva, A.S. Rangwala, and G. Jomaas. "Convection-driven melting in an n-octane pool fire bounded by an ice wall, *Combustion and Flame*" 179:219-227. <https://doi.org/10.1016/j.combustflame.2017.02.006>, 2017.

Fingas, M. "Oil Spill Science and Technology". 2nd ed. Gulf Professional Publishing, 1078 pp, 2016.

Garo, J.P., J. P. Vantelon, S. Gandhi, and J. L. Torero. "Determination of the Thermal Efficiency of Pre-boilover Burning of a Slick of Oil on Water." *Spill Science & Technology Bulletin*, 5(2): 141-151, 1999.

NORCOR. "The interaction of crude oil with Arctic sea ice". Beaufort Sea Technical Report No. 27. Beaufort Sea Project, Department of the Environment, Victoria, BC, Canada. 201 pp, 1975.

Owens, E.H., L.B. Solsberg, and D.F. Dickins. "Field Guide for Oil Spill Response in Arctic Waters". 2nd ed. Emergency Prevention, Preparedness, and Response project, Arctic Council Secretariat, 443 pp, 2017.

Shi, X., R.T. Ranellone, H. Sezer, N. Lamie, L. Zabilansky, K. Stone, and A.S. Rangwala. "Influence of ullage to cavity size ratio on in-situ burning of oil spills in ice-infested water". *Cold Regions Science and Technology*, 140:5-13. <https://doi.org/10.1016/j.coldregions.2017.04.010>, 2017.

Figures



Figure 1 Overview of the burn experiment with ice pan and burning oil pool in the center.

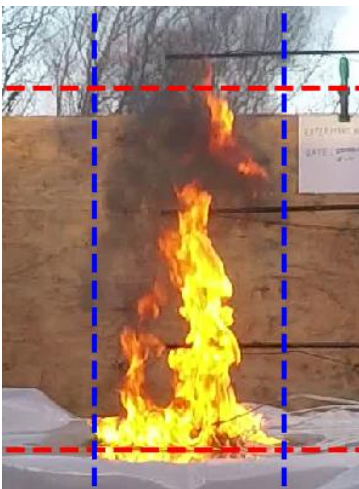


Figure 2 Illustration of automatically derived width (blue lines) and height (red lines) of the flame.

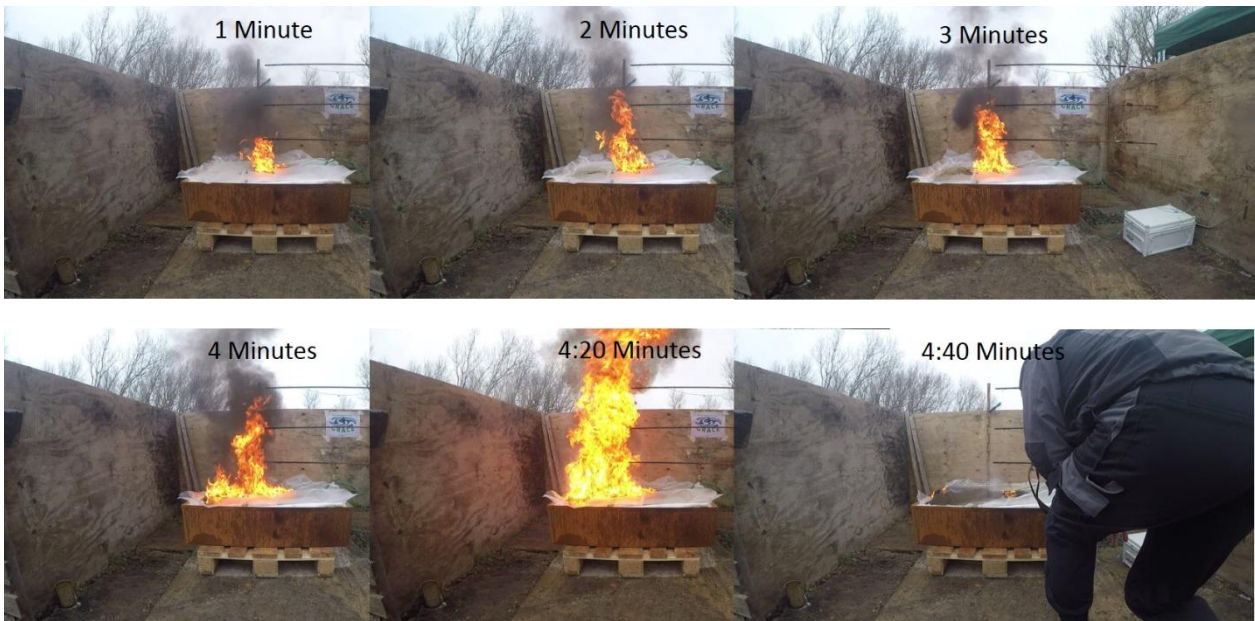


Figure 3 Composite of burn 180321-1 tracing the development of the burn.

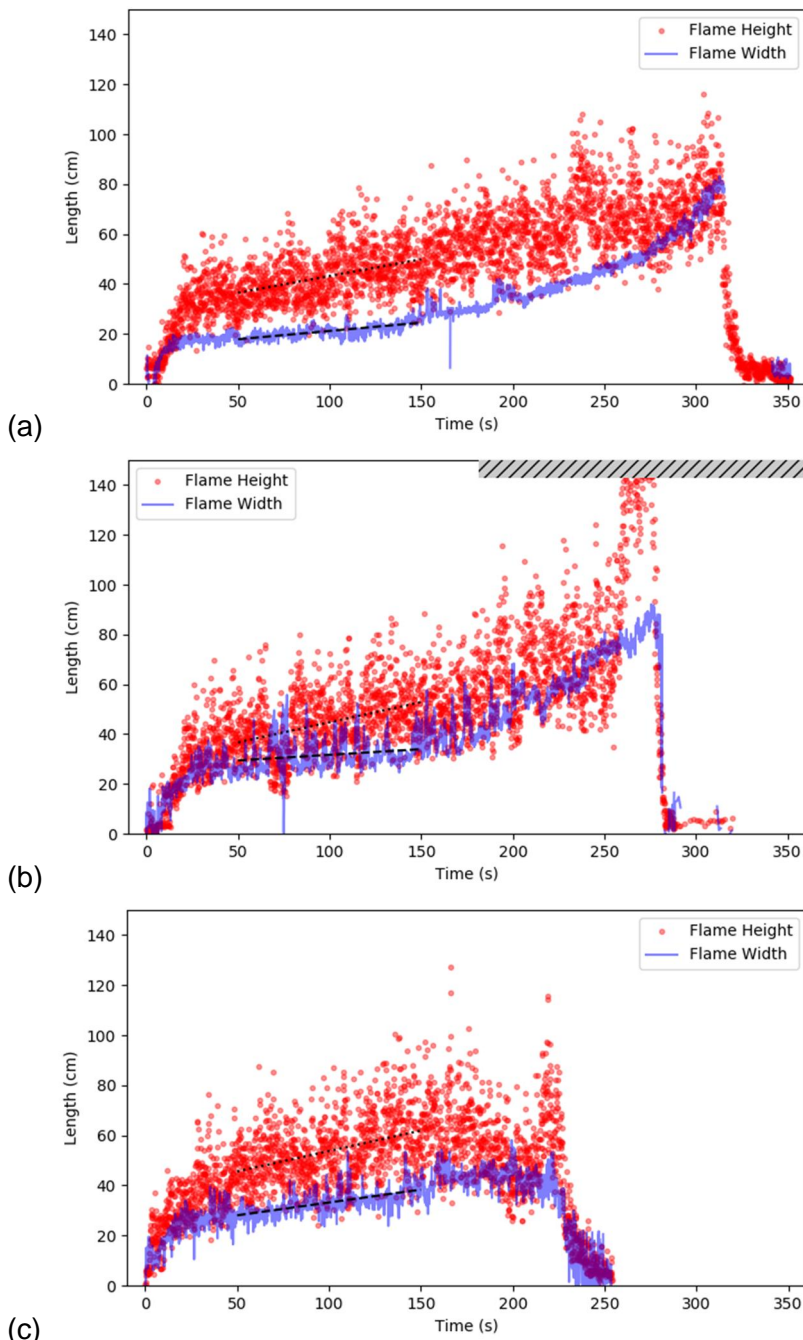


Figure 4 Development of flame height and flame width right above the surface in burns (a) 171015-2, (b) 180321-1, and (c) 180321-2. In (b), the the flame height exceeded the field of view of the camera (hatched area). The dashed and dotted lines are best fit lines with slopes given in Table 2.

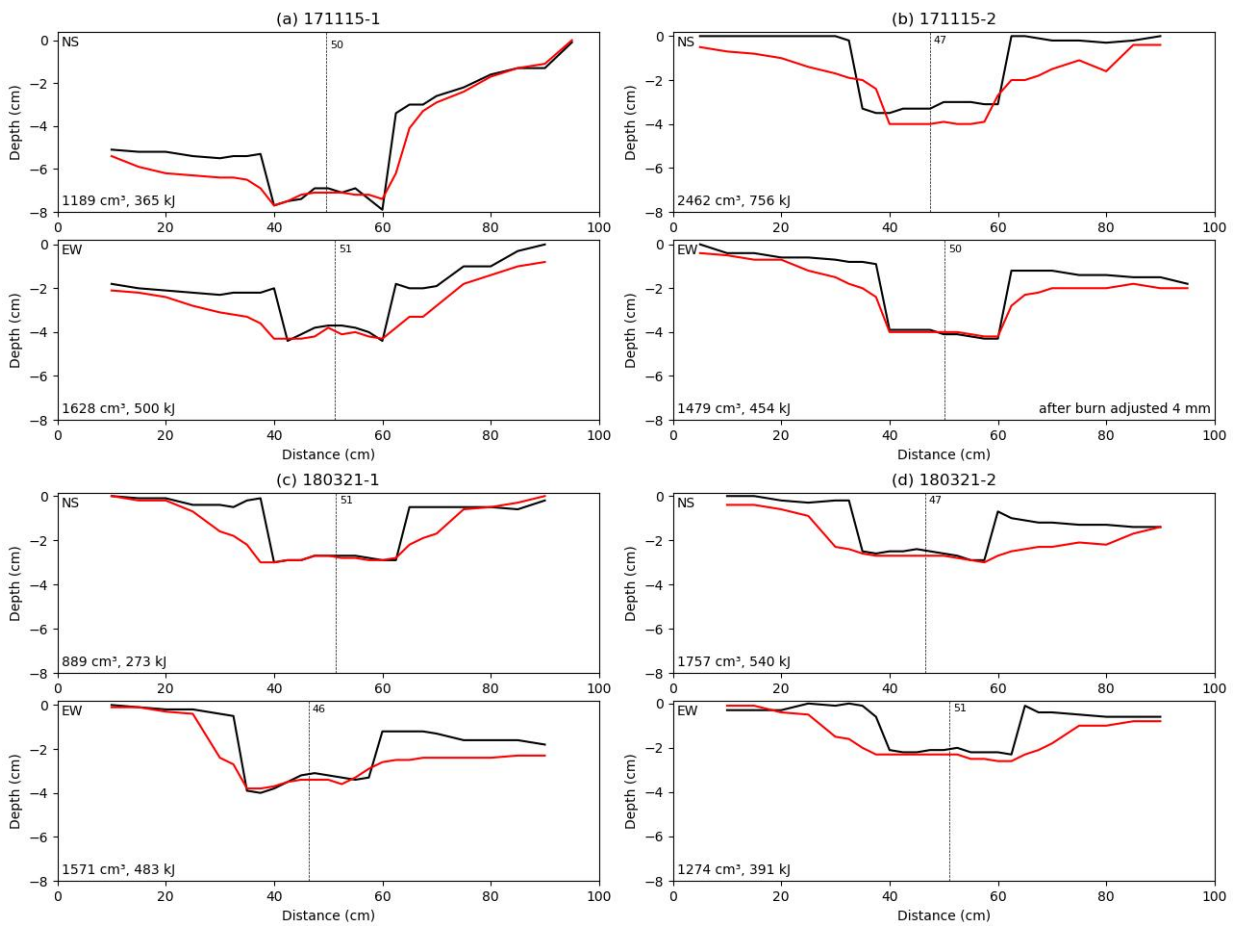


Figure 5 Ice surface profiles before (black lines) and after (red lines) burns (a) 171115-1, (b) 171115-2, (c) 180321-1, (d) 180321-2 for North-South transect (marked NS) and East-West transect (marked EW). Note that scales on the respective axes differ.

Tables

Table 1 Key parameters of experimental burns

Burn	Ambient Temperature (°C)	Pool Size (m)	Oil Mass (g)	Residue Mass (g)	Burn Time (min)	Pool Thickness (mm)	Burn Efficiency (mass %)
171024	11	0.2	357	-*	1:50*	13	-
171115-1	10	0.2	424	201	4:00	16	53
171115-2	9	0.2	708	323	5:20	27	54
171116-1	7	0.2	496	-*	-*	19	-
171116-2	8	0.2	326	212	4:00 [§]	12	35
180321-1	3	0.3	807	289	4:30	14	64
180321-2	3	0.3	484	281	3:50	8	42

* incomplete burn due to run-off of oil
[§] approximately

Table 2 Derived results of burn experiments. Burns 171024 and 171116-1 experienced run-off of oil

Burn	Early Lateral Spread (cm/min)	Early Height Increase (cm/min)	Total Ablation (cm ³)	Enthalpy in Ablation (kJ)	Sensible Flux into Ice (W/m ²)	Fitted Pool Spread Rate _w (cm/min)	Fitted Burn Rate _v (mm/min)
171024	-	-	-	-	-	-	-
171115-1	-*	-*	2800	865	630	6.2	0.8
171115-2	4.0	8.0	- [§]	- [§]	10	7.0	0.7
171116-1	-	-	-	-	-	-	-
171116-2	-*	-*	- [§]	- [§]	- ⁺	6.4	0.4
180321-1	2.7	9.7	2500	756	660	5.6	1.0
180321-2	6.1	9.8	3000	931	940	5.9	0.4

* video footage unsuitable

[§] surface profile measurements not aligned or incomplete

⁺ ice temperature measurements incomplete

Supplementary information

Background

In situ burning is one of the countermeasures available for responding to oil spills in marine but also in other environments e.g. ice/snow, freshwater, marshes. During an in situ burning operation the oil is ignited on the sea surface and through this burning, the oil volume is substantially reduced. The method has been hardly ever used, until 2010 during the Deepwater Horizon incident in the Gulf of Mexico, where between 220,000 and 310,000 barrels of oil were burned during more than 400 burns (Mabile 2012). In situ burning has also been found to be an effective measure for oil spills in Arctic ice filled conditions (e.g. Sørstrøm et al. 2010).

The principle behind *in situ* burning is that the spilled oil is ignited directly on the spill site. To do so, it requires oxygen, a thick (> 1 cm) and relatively fresh oil slick and an igniter that is able to heat the oil to its fire point. The fire point is the temperature where the oil is warm enough to release sufficient vapours to maintain continuous burning (as burning is related to the vapour phase) and typically a few degrees above the flash point (Buist et al. 2013). The oil is thickened by either fire-resistant booms or in ice conditions the ice can act as the containment. Chemical herding agents have also been shown to be able to contract the oil to ignitable thicknesses.

The present measurements are designed to measure the energy feedback from the flame into the ice. The technical background of the experiments was summarized by Fritt-Rasmussen and Petrich (2017). Measurement of energy transfer is achieved by means of temperature measurements in the oil, meltwater, and ice during the burn, and measurements of surface ablation of the ice. This report is on experiences of a dry run (i.e., without ignition) and the first test burn performed in October 2017. The final experiments are set to take place in spring 2018.

Methods

Ice Preparation

Ice was grown in slanted metal pans 1.0 x 1.0 m x 0.3 m, filled with tap water to 0.05 m below the upper rim. A thermocouple probe was built from high-temperature K-Type thermocouple (TC) wire with a vertical arrangement of TCs placed at the center of the tank. The TCs were held in place by feeding them through horizontal holes in a vertical support wooden support pole. TCs that were supposed to record temperatures in the ice were mounted before the probe was installed in the water with the remaining TCs mounted after ice formation shortly before the burn. The wires of the ice TCs were routed along the bottom of the tank to the edge where they left the tank at the surface (Figure 1).

In order to obtain a circular oil pan with well-defined edges, a rubber baking form was added into the water surface prior to onset of freezing. A hole was cut in the center of the form to allow the temperature support pole to penetrate. The form, including the containing ice, was easily removed after ice formation (Figure 2).

Ice was grown at -20 °C air temperature in a commercial refrigeration cargo container (cf. Figure 1).

After removal of the form, thermocouples were inserted into the support through pre-drilled holes. These TCs covered the range through the thickness of the oil lens into the air above (Figure 3). Additional thermocouples were mounted higher above the oil pan from sideways support poles in order to record flame temperatures.



Figure 1. Simultaneous ice growth for multiple experiments in the cold room. Wires of the thermocouples measuring ice temperatures (green) can be seen to emerge at the left hand side of the tanks.



Figure 2. Oil pool depth and diameter were defined by a rubber baking form frozen into the ice at the surface. The form was easily removed from the ice at the beginning of the experiment.



Figure 3. The thermocouples intended to record temperatures above the original ice interface were

placed into the probe support just prior to the start of the experiment. Insert: close-up of the thermocouples protruding from the support.

Experiment Setup

Burn experiments take place outdoors in a sheltered area. Wind and spray protection is installed to a height of 1.5 m at three sides (Figure 4) while the 4th side is protected by a container located 5 m from the pool. A weather station (wind, temperature, pressure) is located at 2.2 m above ground, 2 m from the burn site (Figure 4). The multiplexer for the temperature sensors is placed in a box inside the shelter while the data logger itself is located behind the shelter.



Figure 4. Experiment set-up during dry run on 6 October 2017. The weather station can be seen behind the shelter, slightly to the right of the “Grace” sign. A camera set up to record the burn is seen in the front right of the photo.

Data Acquisition

Data were logged with a battery-powered Campbell Scientific (CS) data logger CS1000 and a CS AM25T multiplexer to measure up to 25 thermocouple temperatures. In addition, the logger recorded weather data from an integrated Vaisala weather transducer, including air temperature, relative humidity, precipitation, wind speed and direction, and air pressure. The recording interval was 10 seconds and recording was started once all thermocouples were in place.

Experiment Timing

The burn experiments are located at the Aarhus University facilities in Roskilde. The campus is shared with atmospheric research groups so that care needs to be taken to perform burn experiments only during suitable wind conditions. In particular, winds should come from easterly directions. On 6 October 2017, a “dry-run” of the experiment was performed but oil had not been ignited due to adverse wind direction. However, wind conditions were favourable on 24 October when a burn had been performed (Figure 5).

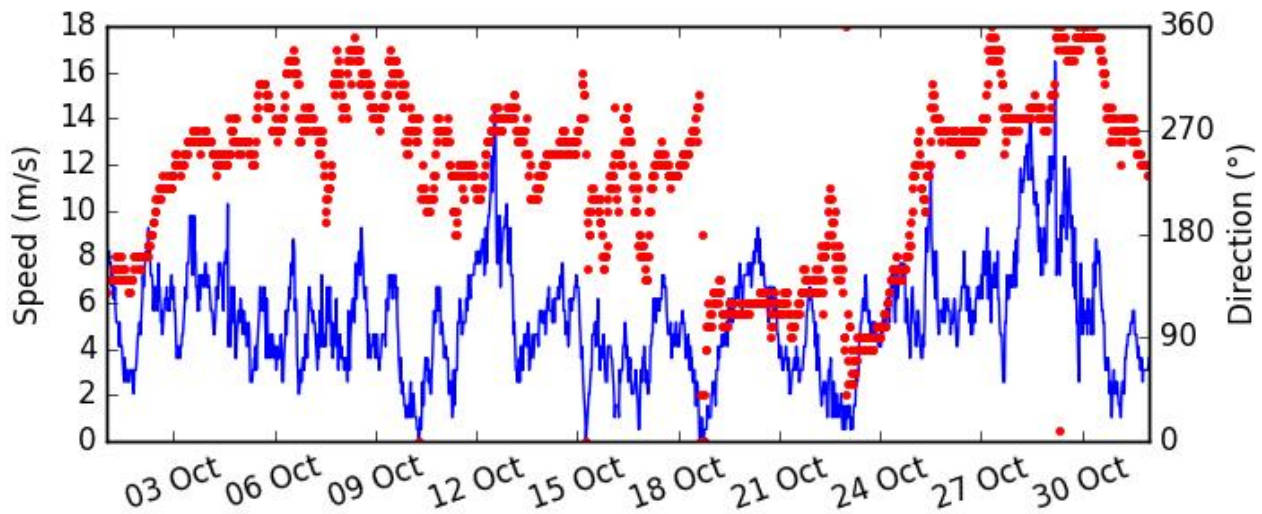


Figure 5. Wind speed (blue line) and direction (red dots) measured at Roskilde airport in October 2017.

Ignition

Oil had been tapped from an outdoor drum holding Troll B crude oil and transported in an air-tight container to the burn site. Oil had been poured into the ice pan and ignited. The time between the end of pouring oil and ignition was approximately 1 minute.

Oil was ignited by a blow torch pointed down at the oil pool such as to avoid melt of surrounding ice by the flame (Figure 6).



Figure 6. Ignition of the oil pool. Photo of 15 Nov 2017, experiment 2.

Surface Profile

The ice surface profile was measured just prior to the burn and after removal of the oil residue following the burn (Figure 7).

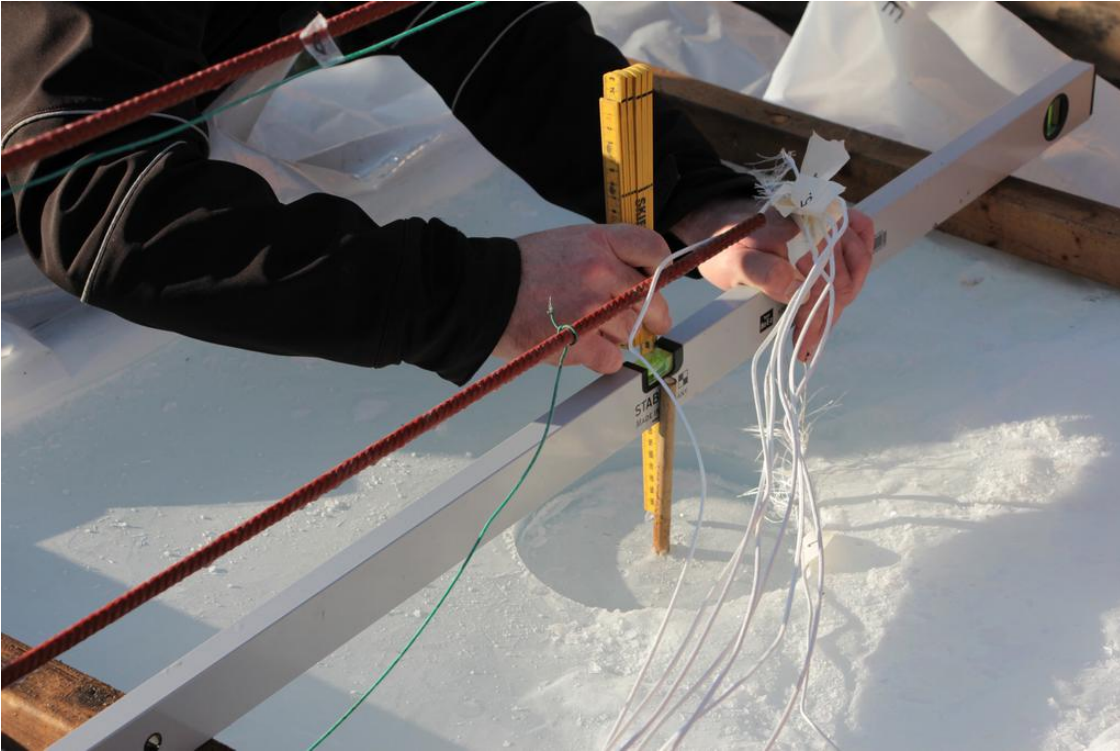


Figure 7. Surface profile measurement before the introduction of oil. Experiment 1 of 15 Nov 2017.

Oil Residue

The original mass of oil and the mass of the oil residue after the burn was measured. Residue oil was collected with pre-weighted absorption pads.

Flame Geometry

The burn was recorded by a GoPro camera to allow for the determination of flame dimensions, in particular flame width above the oil pond and height (Figure 4).

Results and Discussion

The surface of the freshwater ice cover grown in October was cracked as a result of buckling which allowed some oil to drain out of the burn pan, reducing the actual burn time significantly. This was addressed in later experiments in November by introducing a pressure release mat on the inside walls of the tank (cf. ice cover in Figure 7).

The measurement period on 24 October lasted from 13:55:00 when all thermocouples were connected until 14:13:40 when the logger was turned off. The actual burn lasted from 14:05 until 14:07 (Figure 8). Figures 8 to 11 give an overview of the temperature measurements, Table 1 summarizes basic measurements.

As seen in Figure 9, there are two distinct burn periods with recorded peak temperatures between 400 and 450 °C. This was due to turning winds.

As seen in Figure 10, the upper-most temperature sensor in the ice, T(12), melted out shortly after ignition and failed for much of the remaining burn period only to recover to reasonable readings once the flames extinguished. The final temperature suggests that the sensor was in air. Operational failure seems to have taken place at the time the ice melted. The next deeper sensor in the ice, T(11), reached 0 °C quickly (+2 °C for one measurement) and stabilized at 0 °C through the end of the experiment. I.e., it probably remained frozen for the duration of the experiment. The third sensor in the ice, T(10), appears to show temperature increase responding to the 0 °C “boundary” at T(11). Lower temperature sensors in the ice showed a temperature increase that was most likely due to conductive heat transfer in response to surface warming from T(11) (Figure 11).

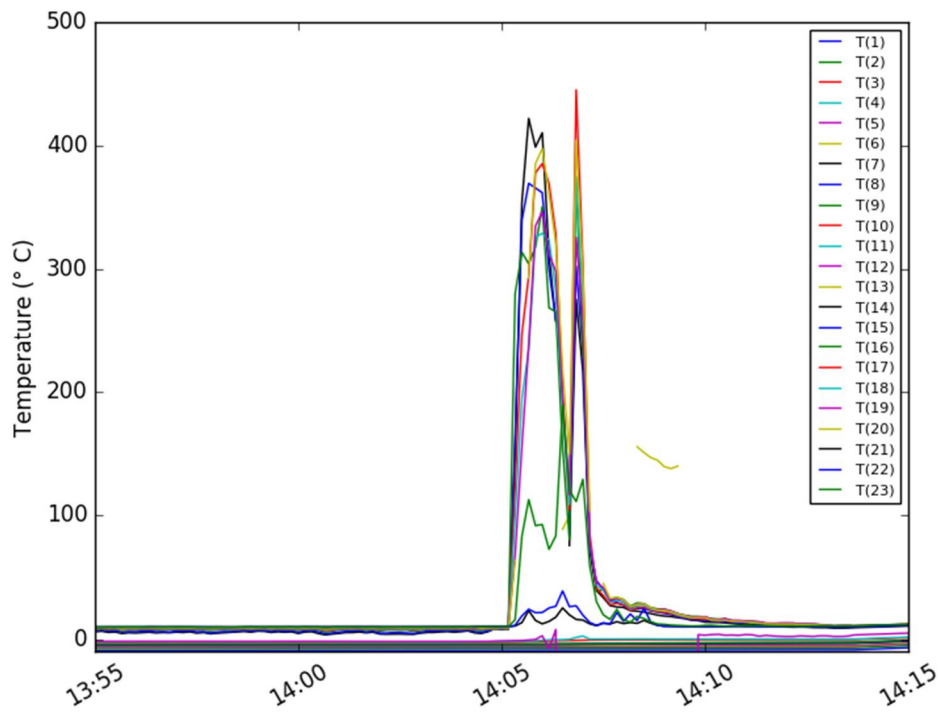


Figure 8. Overview of temperature measurements. T(1) through T(12) are in the ice, cf. Table 1.

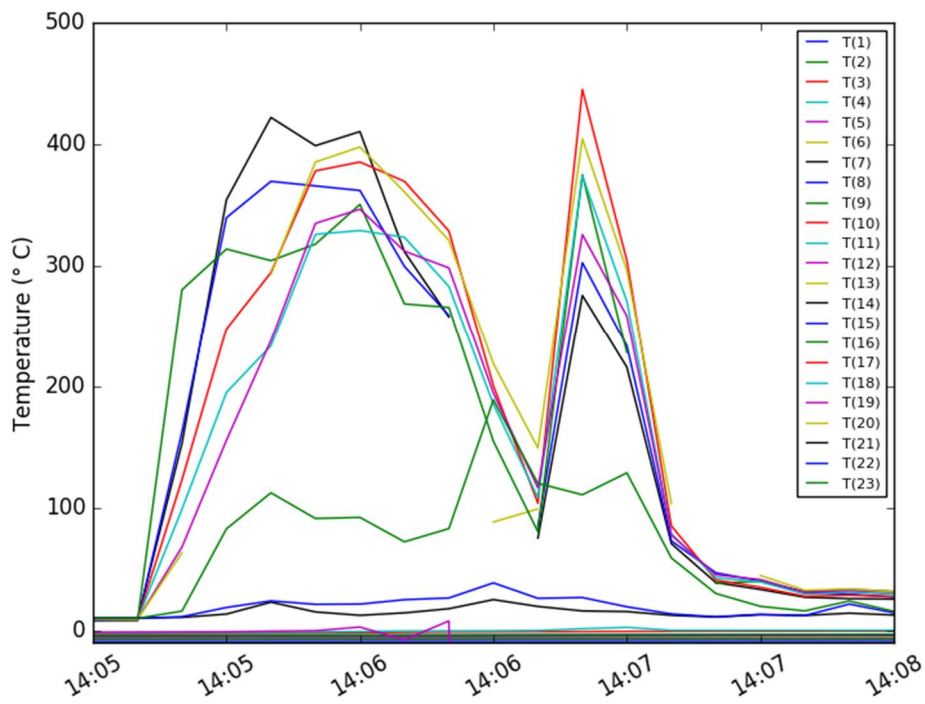


Figure 9. Enlargement to show flame temperature development.

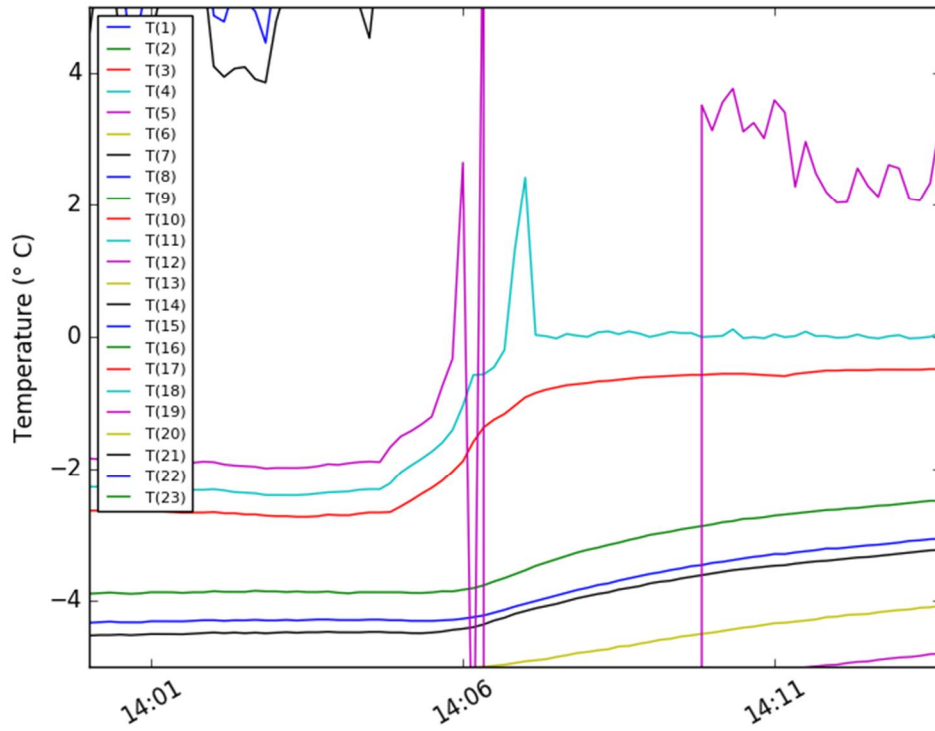


Figure 10. Enlargement to show temperature development in the upper ice layer. T(10) and T(11) are shown in red and cyan, respectively.

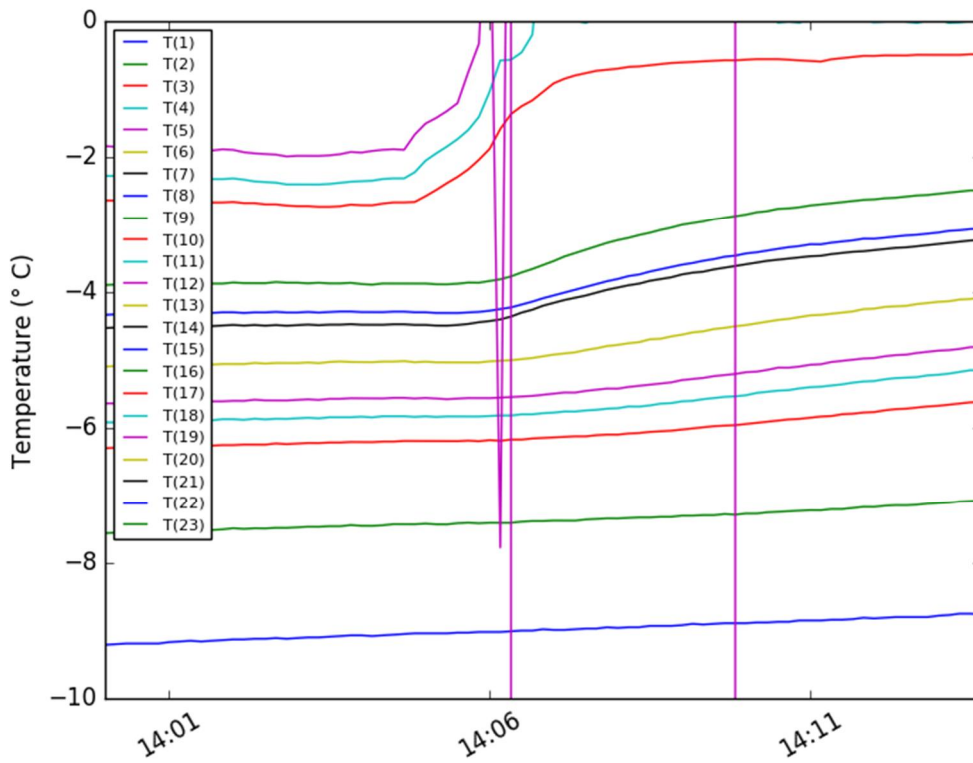


Figure 11. Enlargement to show temperature development in the lower ice layer.

Table 1. Temperatures registered by the thermocouples

Sensor	Initial Temperature 14:00:00	Maximum Temperature	Final Temperature 14:13:40	Comment
T(1)	-9.2 °C	-8.8 °C	-8.8 °C	Ice (lowest/bottom)
T(2)	-7.6 °C	-7.1 °C	-7.1 °C	Ice
T(3)	-6.3 °C	-5.6 °C	-5.6 °C	Ice
T(4)	-5.9 °C	-5.2 °C	-5.2 °C	Ice
T(5)	-5.6 °C	-4.8 °C	-4.8 °C	Ice
T(6)	-5.1 °C	-4.1 °C	-4.1 °C	Ice
T(7)	-4.5 °C	-3.2 °C	-3.2 °C	Ice
T(8)	-4.3 °C	-3.1 °C	-3.1 °C	Ice
T(9)	-3.9 °C	-2.5 °C	-2.5 °C	Ice
T(10)	-2.6 °C	-0.5 °C	-0.5 °C	Ice
T(11)	-2.3 °C	2.4 °C	0.1 °C	Ice
T(12)	-1.8 °C	7.7 °C	3.3 °C	Ice (highest)
T(13)	(no reading)	155.8 °C	(no reading)	Pool (defective)
T(14)	4.5 °C	422.2 °C	9.2 °C	Pool
T(15)	5.5 °C	369.7 °C	9.7 °C	Pool
T(16)	7.0 °C	375.1 °C	10.4 °C	Flame, center
T(17)	7.7 °C	445.2 °C	10.6 °C	Flame, center
T(18)	7.9 °C	374.3 °C	10.6 °C	Flame, center
T(19)	8.2 °C	346.8 °C	10.8 °C	Flame, center
T(20)	8.6 °C	404.7 °C	10.6 °C	Flame, side
T(21)	9.9 °C	25.2 °C	10.2 °C	Flame, side
T(22)	9.6 °C	39.0 °C	10.2 °C	Flame, side
T(23)	9.5 °C	189.5 °C	10.7 °C	Flame, side
T(24)	4.6 °C	8.0 °C	3.9 °C	Spare
T(25)	14.6 °C	17.4 °C	11.4 °C	Spare

Lessons Learned for Main Experiments

General

All technical aspects of the experiment worked as planned with the exception of the ice interface topography.

Ice Interface

The major issue uncovered in the preliminary burn was the generation of a flat ice cover. Volume expansion of ice during formation and thermal contraction of the surrounding basin acted to exert stress on the ice that led to buckling and crack formation. This problem had been successfully addressed prior to the burns in November by using cushioning on the inside of the tank, allowing ice to expand and the surface to remain flat.

References

Buist, I. A, Potter, S.G., Trudel, B.K., Shelnutt, S.R., Walker, A.H., Scholz, D.K., Brandvik, P.J., Fritt-Rasmussen, J., Allen, A.A., and Smith, P. (2013) In Situ Burning in Ice-Affected Waters: State of knowledge report. Final report 7.1.1. Report from Arctic Oil Spill Response Technology Joint Industry Programme (JIP). p. 1-294.

Fritt-Rasmussen, J., and C. Petrich (2017), Literature review report of oil in ice, Integrated oil spill response actions and environmental effects (GRACE), Report D4.1, 27 pp.

Mabile, N. (2012) Controlled In Situ Burning: Transition from Alternative Technology to Conventional Spill Response Option. In: Proceedings of the 33rd Arctic and Marine Oilspill Program (AMOP) Technical Seminar. Environment Canada, Ottawa, ON, Canada, p. 584.

Sørstrøm, S.E., Brandvik, P.J., Buist, I., Daling, P., Dickins, D., Faksness, L.-G., Potter, S., Fritt-Rasmussen, J. and Singaas, I. (2010) Joint industry program on oil spill contingency for Arctic and ice covered waters, Summary report. SINTEF Materials and Chemistry, Marine Environmental Technology report no. A14181.